

Ordered states in AB bilayer graphene in SU(4)-symmetric model

A.V. Rozhkov,¹ A.O. Sboychakov,¹ and A.L. Rakhmanov¹

¹*Institute for Theoretical and Applied Electrodynamics,
Russian Academy of Sciences, 125412 Moscow, Russia*

(Dated: November 5, 2024)

We apply SU(4)-symmetric model to examine possible ordered states in AB stacked bilayer graphene (AB-BLG). The Hamiltonian of the system possesses this symmetry under certain assumptions. In such a model the multicomponent order parameter can be presented as a 4×4 matrix \hat{Q} . Using a mean field approximation, we derive a self-consistency equation for \hat{Q} . Among possible solutions of the obtained equation there are anomalous quantum Hall states, spin, charge, isospin (or valley) density waves, inter-layer excitonic phases and their combinations. We argue that the proposed approach is a useful tool for classification of the ordered states in AB-BLG. The ordered states of the SU(4)-symmetric model demonstrate extensive degeneracies. They can be removed by taking into account the neglected terms, doping, disorder, substrate, as well as other perturbations. The ordered states have varying sensitivity to these factors. This suggests that, for AB-BLG, a ground state ordering type is a non-universal property, susceptible to particulars of extrinsic conditions.

I. INTRODUCTION

The electronic ordered states of graphene-based bilayer systems are studied in a number experimental and theoretical research papers. The reason of such an interest is a richness of the phase diagrams of these materials. Indeed, a number of the ordered phases were observed and/or theoretically predicted in the bilayers. Among them are magnetic¹⁻⁶, “correlated”-insulator⁷⁻⁹, fractional-metal¹⁰⁻¹⁴, superconducting^{3,8,11,15}, and excitonic¹⁶ states. They can be both uniform and inhomogeneous¹⁷⁻²⁰. It is also important that the free energy differences between these numerous phases are small compared to a characteristic energy scale of the electronic system. As a result, the question about the “true” ground state hung in the air since the answer strongly depends on the details of a particular problem, e.g., substrate, sample quality, doping, etc. Moreover, externally-driven cascades of the phase transitions were observed experimentally^{10,12} in AB-stacked bilayer graphene (AB-BLG).

In this situation, it is useful to develop a reasonably general classification scheme that allows one to itemize possible ordered phases in a specific material. In Ref. 21 a symmetry-based analysis of competition between different non-superconducting gapped states in AB-BLG was proposed. The mean field ordered states were classified with the help of a “hidden” SU(4) symmetry. [The emergence of such an extensive symmetry group in the model is a consequence of the SU(2) spin-rotation invariance enhanced by the well-known valley degeneracy, a common feature²²⁻²⁴ for various graphene-based systems.] The introduced multicomponent order parameter can be presented as a 4×4 matrix \hat{Q} , which satisfies a self-consistency equation. The solutions to the self-consistency equation can be grouped according the value of a topological invariant defined in Ref. 21 under assumption of the matrix \hat{Q} being Hermitian.

Similar SU(4)-symmetric model for AA-stacked bilayer graphene (AA-BLG) has been proposed and studied in

our paper Ref. 24 using a mean field approach. We argued that the matrix order parameter \hat{Q} does not have to be Hermitian, and the self-consistency equation allows for non-Hermitian solutions as well.

Given the success of SU(4)-symmetric model for analysis of the AA-BLG ordered phases and certain inconsistencies between the conclusions of Refs. 21 and 24, not to mention an obvious fact that AB-BLG is much better explored experimentally, we believe it is warranted to re-examine the SU(4)-symmetric model for AB-BLG. This is the main goal of this paper.

In our investigation, we identify two types of interaction contributions, direct and umklapp, that are consistent with the SU(4) group. This is to be contrasted with Ref. 21, where a simpler Hamiltonian, with a single coupling constant, was employed. The SU(4)-invariant Hamiltonian is then analyzed within the mean field approach, and a self-consistency equation for the matrix order parameter \hat{Q} is derived. Curiously, the self-consistency equation for the AB-BLG is mathematically identical to that for the AA-BLG obtained in Ref. 24. However, because of dissimilar crystal structures, the AB-BLG effective coupling constants differ from the coupling constants for the AA-BLG.

Here, not only the matrix self-consistency equation generalizing the equation of Ref. 21 is derived but a broader set of solutions is also found. Specifically, in addition to purely Hermitian \hat{Q} , non-Hermitian solutions are explicitly constructed and discussed. Beside this, the topological classification of the order parameters^{21,24} is extended to some non-Hermitian solutions. A number of phases, such as spin and charge-density wave orders, inter-layer excitonic orders, as well as others, can be described by the proposed mean field approach.

The paper is organized as follows. In Sec. II, we derive an approximate SU(4)-symmetric Hamiltonian for the AB-BLG. In Sec. III, we apply the mean-field approach and obtain a self-consistency equation for the multicomponent order parameter \hat{Q} . Possible types of the ordered states in the AB-BLG are analyzed and the obtained re-

sults are discussed in Sec. IV. In Sec. V we summarize the obtained results.

II. TIGHT-BINDING SU(4) SYMMETRIC HAMILTONIAN FOR AB-BLG

A. Single-electron Hamiltonian

The unit cell of the AB-BLG contains four carbon atoms located in two different layers and two different sublattices A and B . The commonly used tight-binding Hamiltonian²⁵ for AB-BLG reads as

$$\hat{H}_0 = \begin{pmatrix} 0 & 0 & -tf(\mathbf{k}) & 0 \\ 0 & 0 & t_0 & -tf(\mathbf{k}) \\ -tf^*(\mathbf{k}) & t_0 & 0 & 0 \\ 0 & -tf^*(\mathbf{k}) & 0 & 0 \end{pmatrix}, \quad (1)$$

where $t \approx 2.7\text{eV}$ is the intralayer nearest-neighbor hopping amplitude, $t_0 \approx 0.35\text{eV}$ is the hopping amplitude between nearest ('dimer') atoms in different layers,

$$f(\mathbf{k}) = 1 + 2 \exp\left(\frac{3ia_0k_x}{2}\right) \cos \frac{\sqrt{3}a_0k_y}{2}, \quad (2)$$

and $a_0 = 1.42\text{\AA}$ is the in-plane carbon-carbon distance. The wave functions of this Hamiltonian are bispinors

$$\hat{\Psi}_{\mathbf{k}\sigma} = (d_{\mathbf{k}1A\sigma}, d_{\mathbf{k}2A\sigma}, d_{\mathbf{k}1B\sigma}, d_{\mathbf{k}2B\sigma})^T, \quad (3)$$

whose components $d_{\mathbf{k}l a \sigma}$ are the second-quantization operators for electrons with momentum \mathbf{k} , in the layer $l = 1, 2$, on the sublattice $a = A, B$, and with spin projection $\sigma = \uparrow, \downarrow$. We neglect here the effect of the trigonal warping arising if we take into account a non-dimer interlayer hopping.

The spectrum of the Hamiltonian (1) consists of four bands $\varepsilon^{(s)}(\mathbf{k})$, where the band index is $s = 1, 2, 3, 4$. Using $\varepsilon^{(s)}$, one can formally diagonalize the Hamiltonian (1)

$$\hat{H}_0 = \sum_{\mathbf{k}, s, \sigma} \varepsilon^{(s)}(\mathbf{k}) \gamma_{\mathbf{k}s\sigma}^\dagger \gamma_{\mathbf{k}s\sigma}. \quad (4)$$

In this formula $\gamma_{\mathbf{k}s\sigma}$ are band operators. Although, explicit expressions for $\varepsilon^{(s)}(\mathbf{k})$ are known²⁵, they are too complicated for our purposes. Instead, we will use the following approximate formulas

$$\varepsilon^{(1,4)}(\mathbf{q}) = \pm [t_0 + \varepsilon_0(\mathbf{q})], \quad \varepsilon^{(2,3)}(\mathbf{q}) = \pm \varepsilon_0(\mathbf{q}), \quad (5)$$

which are valid when $\varepsilon_0 < t_0$ or $|\mathbf{q}| < q_0$, where $q_0 = 2t_0/3ta_0 \approx 0.08a_0^{-1}$, and $\mathbf{q} = \mathbf{k} - \mathbf{K}_\xi$ is the momentum measured relative Dirac point \mathbf{K}_ξ located at

$$\mathbf{K}_\xi = \frac{2\pi}{3\sqrt{3}a_0}(\sqrt{3}, \xi), \quad \text{where } \xi = \pm 1 \quad (6)$$

is the Dirac cone number or valley index, and

$$\varepsilon_0(\mathbf{q}) \approx \frac{9t^2}{4t_0} a_0^2 |\mathbf{q}|^2 = t_0 \frac{|\mathbf{q}|^2}{q_0^2}. \quad (7)$$

Equations (5) demonstrate that bands $s = 2$ and $s = 3$ touch each other at two Dirac points, forming (at zero doping) two Fermi points.

As usual for graphene-based systems, it is convenient to define the Dirac cone index ξ as a valley quantum number characterizing single-electron states. We assign an electron with momentum \mathbf{k} to the valley \mathbf{K}_ξ if $|\mathbf{q}| < q_0$. It is easy to check that $q_0 < |\mathbf{K}_{+1} - \mathbf{K}_{-1}|/2 \approx 1.21a_0^{-1}$ since $t_0/t < 1$. This guarantees that the valleys do not overlap (a state with a given momentum never belongs to both valleys at once). As for the electron states that do not reside in any of the valleys, they are discarded since their contribution to the low-energy physics is insignificant.

It follows from Eqs. (5) that $|\varepsilon^{(2,3)}(q_0)| \leq |\varepsilon^{(1,4)}(\mathbf{q})|$ and we can exclude bands $s = 1, 4$ from our low-energy treatment. This reduces the formulated above tight-binding approach to a generally accepted two-bands effective model²⁵ for AB-BLG. In this case the Hamiltonian (4) reads

$$\hat{H}_0^{\text{eff}} = \sum_{\mathbf{q}, \xi, \sigma} \varepsilon_0(\mathbf{q}) \left(\gamma_{\mathbf{q}2\xi\sigma}^\dagger \gamma_{\mathbf{q}2\xi\sigma} - \gamma_{\mathbf{q}3\xi\sigma}^\dagger \gamma_{\mathbf{q}3\xi\sigma} \right). \quad (8)$$

Here the relations between the valley-specific band operators $\gamma_{\mathbf{q}s\xi\sigma}$ and valley-specific lattice operators $d_{\mathbf{q}l a \xi \sigma}$ in the main approximation in $q/q_0 < 1$ can be presented in the form

$$\begin{aligned} d_{\mathbf{q}1A\xi\sigma} &= \frac{e^{i\xi\phi_{\mathbf{q}}}}{\sqrt{2}} (-\gamma_{\mathbf{q}2\xi\sigma} + \xi\gamma_{\mathbf{q}3\xi\sigma}), \\ d_{\mathbf{q}2B\xi\sigma} &= \frac{e^{-i\xi\phi_{\mathbf{q}}}}{\sqrt{2}} (\gamma_{\mathbf{q}2\xi\sigma} + \xi\gamma_{\mathbf{q}3\xi\sigma}), \end{aligned} \quad (9)$$

where $\exp(i\phi_{\mathbf{q}}) = -(iq_x + q_y)/|\mathbf{q}|$, and $\xi = -1$ ($\xi = 1$) for \mathbf{K}_1 (for \mathbf{K}_2). Deriving these compact expressions we employed the fact that any band operator is defined up to a (undetermined) phase factor, which enables us to fix this phase based on convenience. Note also that in our approximation the dimer sites do not participate in the low-energy electron physics.

In expression (8), the band energies are independent of the spin and valley indices, while different spin projections and different valley indices correspond to different electronic states. We see that the single-electron Hamiltonian \hat{H}_0^{eff} is SU(4) symmetric in the multi-index space $m = (\xi, \sigma)$. That is, \hat{H}_0^{eff} is invariant under Bogolyubov's transformation

$$\gamma_{\mathbf{q}sm} = \sum_{m'} u_{mm'} \gamma_{\mathbf{q}sm'}, \quad (10)$$

where $u_{mm'}$ are matrix elements of a 4×4 unitary matrix.

B. Effective interaction Hamiltonian

The interaction part of the Hamiltonian \hat{H}_{int} is assumed to be spin-independent density-density type²⁴

$$\hat{H}_{\text{int}} = \frac{1}{2N_c} \sum_{\mathbf{k}l'l''} V_{\mathbf{k}}^{ll''} \hat{\rho}_{\mathbf{k}l} \hat{\rho}_{-\mathbf{k}l''}. \quad (11)$$

In this formula N_c is the number of unit cells in the system, \mathbf{k} is a transferred momentum $V_{\mathbf{k}}^{ll''}$ is the Fourier transform of the potential energy $V^{ll''}(\mathbf{r})$ of the interaction between an electron in the layer l and another electron in the layer l'' , and \mathbf{r} is a distance between these electrons. The value $\hat{\rho}_{\mathbf{k}l}$ is the Fourier component of a single-site density operator defined for elementary cell \mathbf{n} as $\hat{\rho}_{\mathbf{n}1} = \sum_{\sigma} d_{\mathbf{n}1A\sigma}^{\dagger} d_{\mathbf{n}1A\sigma}$ and $\hat{\rho}_{\mathbf{n}2} = \sum_{\sigma} d_{\mathbf{n}2B\sigma}^{\dagger} d_{\mathbf{n}2B\sigma}$.

We assume that the interaction is weaker at large transferred momenta and stronger at smaller ones. In particular, $|V_{\mathbf{k}\xi}^{ll''}| < V_{\mathbf{k}}^{ll''}$ for $|\mathbf{k}| < q_0$. In such a situation, one can neglect the so-called backscattering and consider only the case of small $|\mathbf{k}| < q_0$, which guarantees that the scattered electrons remain in their valleys. Thus, we can define a ‘chiral’ components of the density operators

$$\hat{\rho}_{\mathbf{k}1}^{\xi} = \sum_{\mathbf{q}\sigma} d_{\mathbf{q}1A\xi\sigma}^{\dagger} d_{\mathbf{q}+\mathbf{k}1A\xi\sigma}, \quad (12)$$

$$\hat{\rho}_{\mathbf{k}2}^{\xi} = \sum_{\mathbf{q}\sigma} d_{\mathbf{q}2B\xi\sigma}^{\dagger} d_{\mathbf{q}+\mathbf{k}2B\xi\sigma}, \quad (13)$$

and approximate the interaction as

$$\hat{H}_{\text{int}} \approx \frac{1}{2N_c} \sum_{\mathbf{k}\xi\xi'l'l''} V_{\mathbf{k}}^{ll''} \hat{\rho}_{\mathbf{k}l}^{\xi} \hat{\rho}_{-\mathbf{k}l''}^{\xi'}. \quad (14)$$

Finally, disregarding any layer asymmetry we assume that $V_{\mathbf{k}}^{11} = V_{\mathbf{k}}^{22}$, and $V_{\mathbf{k}}^{12} = V_{\mathbf{k}}^{21} < V_{\mathbf{k}}^{11}$.

Introducing linear combinations of the interaction potentials $V_{\mathbf{k}}^{\pm} = V_{\mathbf{k}}^{11} \pm V_{\mathbf{k}}^{12}$, we express Hamiltonian (14) in the following form

$$\hat{H}_{\text{int}} \approx \frac{1}{4N_c} \sum_{\mathbf{k}} (V_{\mathbf{k}}^{+} \hat{\rho}_{\mathbf{k}} \hat{\rho}_{-\mathbf{k}} + V_{\mathbf{k}}^{-} \hat{\chi}_{\mathbf{k}} \hat{\chi}_{-\mathbf{k}}), \quad (15)$$

where

$$\hat{\rho}_{\mathbf{k}} = \sum_{\xi} (\hat{\rho}_{\mathbf{k}1}^{\xi} + \hat{\rho}_{\mathbf{k}2}^{\xi}), \quad \hat{\chi}_{\mathbf{k}} = \sum_{\xi} (\hat{\rho}_{\mathbf{k}1}^{\xi} - \hat{\rho}_{\mathbf{k}2}^{\xi}). \quad (16)$$

We can identify $\hat{\rho}_{\mathbf{k}}$ as electron density operator for the bilayer, while $\hat{\chi}_{\mathbf{k}}$ can be viewed as a dipole-moment density operator. Consequently, $V_{\mathbf{k}}^{+}$ represents the interaction between electric charges, while $V_{\mathbf{k}}^{-}$ describes dipole-dipole interaction.

Using Eqs. (9), (12) and (13) we can express $\hat{\rho}_{\mathbf{k}}$ in terms of the band operators

$$\hat{\rho}_{\mathbf{k}} = \sum_{\mathbf{q}m} \left[\cos \phi_{\mathbf{q}\mathbf{k}} \left(\gamma_{\mathbf{q}2m}^{\dagger} \gamma_{\mathbf{q}+\mathbf{k}2m} + \gamma_{\mathbf{q}3m}^{\dagger} \gamma_{\mathbf{q}+\mathbf{k}3m} \right) \right. \\ \left. + i \sin \phi_{\mathbf{q}\mathbf{k}} \left(\gamma_{\mathbf{q}2m}^{\dagger} \gamma_{\mathbf{q}+\mathbf{k}3m} + \gamma_{\mathbf{q}3m}^{\dagger} \gamma_{\mathbf{q}+\mathbf{k}2m} \right) \right], \quad (17)$$

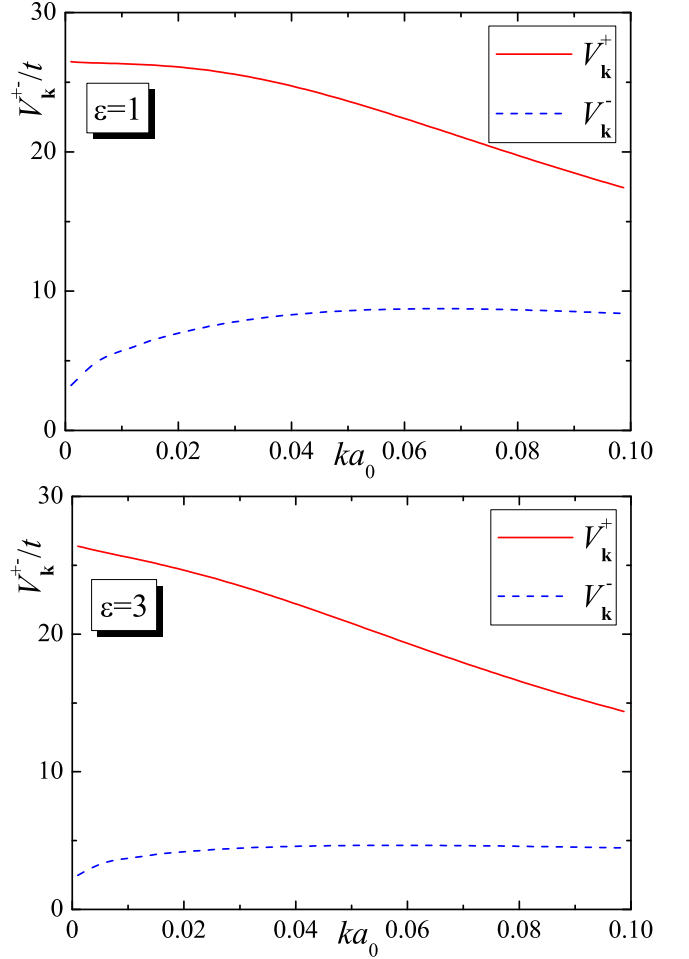


FIG. 1: Effective interactions $V_{\mathbf{k}}^{\pm}$ calculated using the RPA approach for AB-BLG, as in Ref. 15. The panels show the data for two different values of the dielectric constants of the media surrounding the AB-BLG sample: $\varepsilon = 1$ for the top panel and $\varepsilon = 3$ for the bottom panel. Solid (red) curves on both panels represent $V_{\mathbf{k}}^{+}$ as function of transferred momentum \mathbf{k} for $|\mathbf{k}| < q_0$. Dashed (blue) curves represent $V_{\mathbf{k}}^{-}$. Dependence on the direction of \mathbf{k} is weak and may be neglected. For both values of the dielectric constant we can clearly observe that $V_{\mathbf{k}}^{-} < V_{\mathbf{k}}^{+}$.

where $\phi_{\mathbf{q}\mathbf{k}} = \phi_{\mathbf{q}} - \phi_{\mathbf{q}+\mathbf{k}}$. This form explicitly demonstrates that $\hat{\rho}_{\mathbf{k}}$ is SU(4)-invariant operator.

At the same time, the dipole-momentum density operator does not have the same invariance, as one can see from the formula

$$\hat{\chi}_{\mathbf{k}} = -\sum_{\mathbf{q}\xi\sigma} \xi \left[i \sin \phi_{\mathbf{q}\mathbf{k}} \left(\gamma_{\mathbf{q}2\xi\sigma}^{\dagger} \gamma_{\mathbf{q}+\mathbf{k}2\xi\sigma} + \gamma_{\mathbf{q}3\xi\sigma}^{\dagger} \gamma_{\mathbf{q}+\mathbf{k}3\xi\sigma} \right) \right. \\ \left. + \cos \phi_{\mathbf{q}\mathbf{k}} \left(\gamma_{\mathbf{q}2\xi\sigma}^{\dagger} \gamma_{\mathbf{q}+\mathbf{k}3\xi\sigma} + \gamma_{\mathbf{q}3\xi\sigma}^{\dagger} \gamma_{\mathbf{q}+\mathbf{k}2\xi\sigma} \right) \right]. \quad (18)$$

The sign-oscillating factor $\xi = \pm 1$ in this relation explicitly spoils the invariance.

Following Ref. 21, we disregard dipole-dipole interaction $V_{\mathbf{k}}^{-}$ in the Hamiltonian (15) since $V_{\mathbf{k}}^{+} > V_{\mathbf{k}}^{-}$. To

explain this simplification, let us examine Fig. 1. Its two panels present the AB-BLG effective interaction calculated within the random-phase approximation (RPA) framework¹⁵. We see that for both values of the dielectric constant, the latter inequality remains valid in the relevant transferred momenta window $|\mathbf{k}| < q_0$.

Thus, the effective Hamiltonian can be simplified as

$$\hat{H}_{\text{int}} \approx \frac{1}{4N_c} \sum_{\mathbf{k}} V_{\mathbf{k}}^+ \hat{\rho}_{\mathbf{k}} \hat{\rho}_{-\mathbf{k}}. \quad (19)$$

The obtained interaction Hamiltonian is SU(4) invariant. Its SU(4) symmetry, as well as the symmetry of the single-electron Hamiltonian (8), follows from the fact that the band energies $\varepsilon_0(\mathbf{q})$ and the matrix elements $V_{\mathbf{k}}^{ll'}$ are independent of the multi-index m , while bilinears

$$\sum_m \gamma_{\mathbf{q}sm}^\dagger \gamma_{\mathbf{q}'s'm}$$

$$\hat{H}_{\text{int}}^{\text{MF}} = -\frac{1}{2N_c} \sum_{\mathbf{p}\mathbf{q}\mathbf{m}\mathbf{m}'} V_{\mathbf{p}-\mathbf{q}}^+ \langle \gamma_{\mathbf{p}3m}^\dagger \gamma_{\mathbf{p}2m'} \rangle \left[\cos^2(\phi_{\mathbf{q}} - \phi_{\mathbf{p}}) \gamma_{\mathbf{q}2m'}^\dagger \gamma_{\mathbf{q}3m} + \sin^2(\phi_{\mathbf{q}} - \phi_{\mathbf{p}}) \gamma_{\mathbf{q}3m'}^\dagger \gamma_{\mathbf{q}2m} \right] + \text{H.c.} \quad (20)$$

To make the mean-field formulas more transparent, we introduce the 4×4 operator-valued matrix $\hat{\Theta}_{\mathbf{q}}$ whose matrix elements are

$$\Theta_{\mathbf{q}mm'} = \gamma_{\mathbf{q}3m}^\dagger \gamma_{\mathbf{q}2m'}. \quad (21)$$

As a result, we obtain a compact expression for the interaction Hamiltonian in the mean-field approach

$$\begin{aligned} \hat{H}_{\text{int}}^{\text{MF}} &= \hat{H}_{\text{dir}}^{\text{MF}} + \hat{H}_{\text{um}}^{\text{MF}}, \\ \hat{H}_{\text{dir}}^{\text{MF}} &= -\frac{1}{2N_c} \sum_{\mathbf{q}\mathbf{p}} V_{\mathbf{q}\mathbf{p}}^{\text{dir}} \text{Tr} \left(\langle \hat{\Theta}_{\mathbf{p}}^\dagger \rangle \hat{\Theta}_{\mathbf{q}} + \langle \hat{\Theta}_{\mathbf{p}} \rangle \hat{\Theta}_{\mathbf{q}}^\dagger \right), \\ \hat{H}_{\text{um}}^{\text{MF}} &= -\frac{1}{2N_c} \sum_{\mathbf{q}\mathbf{p}} V_{\mathbf{q}\mathbf{p}}^{\text{um}} \text{Tr} \left(\langle \hat{\Theta}_{\mathbf{p}} \rangle \hat{\Theta}_{\mathbf{q}} + \langle \hat{\Theta}_{\mathbf{p}}^\dagger \rangle \hat{\Theta}_{\mathbf{q}}^\dagger \right). \end{aligned} \quad (22)$$

Here

$$\begin{aligned} V_{\mathbf{q}\mathbf{p}}^{\text{dir}} &= V_{\mathbf{q}-\mathbf{p}}^+ \cos^2(\phi_{\mathbf{q}} - \phi_{\mathbf{p}}), \\ V_{\mathbf{q}\mathbf{p}}^{\text{um}} &= V_{\mathbf{q}-\mathbf{p}}^+ \sin^2(\phi_{\mathbf{q}} - \phi_{\mathbf{p}}), \end{aligned} \quad (23)$$

are direct ('dir') and umklapp ('um') interactions. For RPA interaction, the function $V_{\mathbf{q}}^+$ is finite for any \mathbf{q} due to the finite density of states at the Fermi level. This allows us approximate Eq. (22) replacing the functions $V_{\mathbf{q}\mathbf{p}}^{\text{dir}}$ and $V_{\mathbf{q}\mathbf{p}}^{\text{um}}$ by their mean values in the range $|\mathbf{q}| < q_0$,

$$\bar{V}_{\text{dir,um}} = \frac{1}{\pi^2 q_0^4} \int_{\substack{|\mathbf{q}| < q_0 \\ |\mathbf{p}| < q_0}} d^2\mathbf{q} d^2\mathbf{p} V_{\mathbf{q}\mathbf{p}}^{\text{dir,um}}. \quad (24)$$

In essence, this formula is a familiar theoretical device common to numerous BCS-like mean field schemes: detailed interaction function, which is often unknown, is

in Eq. (8) and (17) remain unchanged under the action of the SU(4) Bogolyubov transformation (10).

III. MEAN FIELD APPROACH

Now we apply the mean field approach to the obtained effective Hamiltonian (19). Note that only non-zero averages which couples bands 2 and 3 are of importance since they open a gap in the spectrum of the charge carriers. Then, performing the mean field decoupling and taking into account that $V_{\mathbf{p}-\mathbf{q}}^+ = V_{\mathbf{q}-\mathbf{p}}^+$ we derive

replaced by an effective coupling constant. For RPA interaction at $\varepsilon = 1$, see Fig. 1(top), we estimate

$$\bar{V}_{\text{dir}}/t \approx 9.37, \quad \bar{V}_{\text{um}}/t \approx 8.93. \quad (25)$$

Note that, within our model, the two coupling constants are very close to each other.

With such a replacement, the mean field interaction Hamiltonian can be approximated as

$$\hat{H}_{\text{int}}^{\text{MF}} = -\sum_{\mathbf{q}} \text{Tr} \left(\hat{Q}^\dagger \hat{\Theta}_{\mathbf{q}} + \hat{Q} \hat{\Theta}_{\mathbf{q}}^\dagger \right), \quad (26)$$

where we introduced a matrix order parameter \hat{Q}

$$\hat{Q} = \frac{1}{2N_c} \sum_{\mathbf{p}} \left(\bar{V}_{\text{dir}} \langle \hat{\Theta}_{\mathbf{p}} \rangle + \bar{V}_{\text{um}} \langle \hat{\Theta}_{\mathbf{p}}^\dagger \rangle \right), \quad (27)$$

which is the \mathbf{q} independent in the range $|\mathbf{q}| < q_0$, and equal to zero otherwise. The definition Eq. (27) can be inverted

$$\frac{1}{2N_c} \sum_{\mathbf{p}} \langle \hat{\Theta}_{\mathbf{p}} \rangle = \frac{1}{\bar{V}_{\text{dir}}^2 - \bar{V}_{\text{um}}^2} \left(\bar{V}_{\text{dir}} \hat{Q} - \bar{V}_{\text{um}} \hat{Q}^\dagger \right). \quad (28)$$

In so doing, we have reduced formally the mean-field problem for AB-BLG to the case considered in Ref. 24 for the AA-BLG. Thus, we can use the relation (60) from that paper

$$\sum_{\mathbf{p}} \langle \hat{\Theta}_{\mathbf{p}} \rangle = \frac{1}{2} \sum_{\mathbf{q}} \hat{Q} \left(\varepsilon_0^2(\mathbf{q}) + \hat{Q}^\dagger \hat{Q} \right)^{-1/2} \quad (29)$$

and derive a self-consistency equation in a convenient form

$$(\bar{V}_{\text{dir}}^2 - \bar{V}_{\text{um}}^2) \hat{Q} h(\hat{Q}^\dagger \hat{Q}) = \bar{V}_{\text{dir}} \hat{Q} - \bar{V}_{\text{um}} \hat{Q}^\dagger, \quad (30)$$

where

$$h(\hat{Q}^\dagger \hat{Q}) = \frac{1}{4N_c} \sum_{\mathbf{q}} \left(\varepsilon_0^2(\mathbf{q}) + \hat{Q}^\dagger \hat{Q} \right)^{-1/2}. \quad (31)$$

The matrix $\hat{Q}^\dagger \hat{Q}$ is non-negative Hermitian matrix. We use Hermitian-matrix representation $\hat{Q}^\dagger \hat{Q} = \hat{U} \hat{D}^2 \hat{U}^\dagger$, where \hat{U} is a unitary matrix and

$$\hat{D} = \text{diag}(d_1, \dots, d_4), \quad d_i \geq 0, \quad (32)$$

is a diagonal matrix with positive eigenvalues. As a result, we can write

$$h(\hat{Q}^\dagger \hat{Q}) = \hat{U} h(\hat{D}^2) \hat{U}^\dagger, \quad (33)$$

and

$$h(\hat{D}^2) = \frac{\nu_0}{4} \int_0^{t_0} d\varepsilon \left(\varepsilon^2 + \hat{D}^2 \right)^{-1/2} \approx \frac{\nu_0}{4} \log \left(\frac{2t_0}{\hat{D}} \right), \quad (34)$$

where $\nu_0 = t_0/(2\sqrt{3}\pi t^2)$ is the AB-BLG density of states (per valley per spin projection).

IV. MEAN-FIELD STATES

The mean-field ordered phases of our SU(4)-symmetric Hamiltonian are the solutions of the self-consistency equation (30). It is quite remarkable that the same equation was derived in Ref. 24. for the different type of bilayer, AA-BLG [see Eq. (61) in the latter reference]. This allows us to rely on Ref. 24 for the analysis of Eq. (30).

While the full set of solutions for Eq. (30) is unknown, we can identify several useful subsets. Let us assume that the order parameter matrix \hat{Q} is normal (unitary-diagonalizable), that is, it can be represented as

$$\hat{Q} = \hat{U} \text{diag}(q_1, q_2, q_3, q_4) \hat{U}^\dagger, \quad (35)$$

where \hat{U} is unitary, and q_j are complex $q_j = |q_j| e^{i\phi_j} \in \mathbb{C}$.

Substituting such a matrix into the self-consistency equation, one can establish that $e^{i\phi_j}$ is either ± 1 or $\pm i$. This means that any q_j is either purely real, or purely imaginary. For $|q_j|$ we derive

$$\frac{\nu_0}{4} |q_j| \log \left(\frac{2t_0}{|q_j|} \right) = \frac{|q_j|}{\bar{V}_{\text{dir}} \pm \bar{V}_{\text{um}}}, \quad (36)$$

such that one must choose plus sign (minus sign) for purely real (purely imaginary) q_j .

The latter equation is easy to solve and find that either $q_j = 0$, or

$$q_j = \pm \Delta_+, \quad \text{or } q_j = \pm i \Delta_-, \quad (37)$$

where

$$\Delta_{\pm} = 2t_0 e^{-2/\lambda_{\pm}}, \quad (38)$$

and we defined two dimensionless coupling constants

$$\lambda_{\pm} = \frac{\nu_0}{2} (\bar{V}_{\text{dir}} \pm \bar{V}_{\text{um}}). \quad (39)$$

One can prove that, if \hat{Q} is a solution of Eq. (30), then $\hat{V} \hat{Q} \hat{V}^\dagger$ is also a solution if $\hat{V} \in \text{SU}(4)$. In other words, all matrices that are unitary equivalent to a known solution are solutions themselves. The inverse statement is not true: two solutions to Eq. (30) are not necessary unitary equivalent. For example, if \hat{Q}_1 has one imaginary eigenvalue, while \hat{Q}_2 has none, the two cannot be connected by a unitary transformation. Consequently, the whole subset of mean field order parameters described by Eq. (35) can be split into several SU(4)-multiplets.

The detailed analysis of the mean-field states satisfying the self-consistency equation (30) is already published in Ref. 24. Here we will limit ourselves to a short discussion only.

Two diagonalizable matrices are unitary equivalent only when their eigenvalue sets are identical up to a permutation. This allows us to split all solutions (35) into three groups, which differ in number of real values q_j in the eigenvalue set: (i) all four q_j are real, (ii) all q_j are imaginary. In group (iii) some eigenvalues are real, some are purely imaginary.

Within each of the three groups there are even finer divisions. To illustrate this let us examine group (i) with all real q_j . When all q_j are real, one can use Eqs. (35) and (37) and write

$$\hat{Q} = \Delta_+ \hat{U} \text{diag}(\pm 1, \pm 1, \pm 1, \pm 1) \hat{U}^\dagger. \quad (40)$$

In this expression all four signs are independent of each other and can be chosen arbitrarily.

For matrices of this type, the invariant quantity is the number of positive eigenvalues²¹ (up to overall sign change $\hat{Q} \rightarrow -\hat{Q}$). Thus, we can introduce three classes of such matrices

$$\text{Class I: } \Delta_+ \hat{U} \text{diag}(\kappa, \kappa, \kappa, \kappa) \hat{U}^\dagger, \quad \kappa = \pm 1, \quad (41)$$

$$\text{Class II: } \Delta_+ \hat{U} \text{diag}(1, 1, -1, -1) \hat{U}^\dagger, \quad (42)$$

$$\text{Class III: } \Delta_+ \hat{U} \text{diag}(\kappa, \kappa, \kappa, -\kappa) \hat{U}^\dagger, \quad \kappa = \pm 1. \quad (43)$$

These classes were introduced previously in Ref. 21.

The order parameters from set (i) represent various types of density wave (charge-, spin-, valley-, spin-valley-density wave). Indeed, one can check that

$$\hat{Q} \propto \text{diag}(\pm 1, \pm 1, \pm 1, \pm 1) \quad (44)$$

represents symmetry-breaking contributions to local densities $\langle d_{\mathbf{q}1A\xi\sigma}^\dagger d_{\mathbf{q}1A\xi\sigma} \rangle$ and $\langle d_{\mathbf{q}2B\xi\sigma}^\dagger d_{\mathbf{q}2B\xi\sigma} \rangle$. The signs of the eigenvalues of \hat{Q} are responsible for realization of a specific density-wave type.

The order parameters from set (ii)

$$\hat{Q} = \Delta_- \text{diag}(\pm i, \pm i, \pm i, \pm i) \quad (45)$$

cannot be described as a density wave of any kind. Instead, they represent inter-layer-exciton-type order parameter, as we will see below.

Equation (45) implies that the matrix elements $\langle \gamma_{\mathbf{q}2m}^\dagger \gamma_{\mathbf{q}3m} \rangle = \langle \gamma_{\mathbf{q}3m}^\dagger \gamma_{\mathbf{q}2m} \rangle^*$ are purely imaginary. Consequently, the quantity

$$\mathfrak{E}_{\mathbf{q}m} = i \left(\langle \gamma_{\mathbf{q}2m}^\dagger \gamma_{\mathbf{q}3m} \rangle - \langle \gamma_{\mathbf{q}3m}^\dagger \gamma_{\mathbf{q}2m} \rangle \right) \quad (46)$$

is purely real. The sign of $\mathfrak{E}_{\mathbf{q}m}$ depends on m .

Using Eq. (9), one can express $\mathfrak{E}_{\mathbf{q}m}$ in terms of the \hat{d} -operators

$$\mathfrak{E}_{\mathbf{q}\xi\sigma} = i\xi e^{-2i\xi\phi_{\mathbf{q}}} \langle d_{\mathbf{q}2B\xi\sigma}^\dagger d_{\mathbf{q}1A\xi\sigma} \rangle + \text{C.c.} \quad (47)$$

Thus we see that $\mathfrak{E}_{\mathbf{q}m}$ corresponds to a type of symmetry-breaking inter-layer coupling between a particle in one layer and a hole in the other layer, that is, to an exciton. Curiously, while $\mathfrak{E}_{\mathbf{q}m}$ becomes finite only when a symmetry is broken, the matrix elements $\langle d_{\mathbf{q}2B\xi\sigma}^\dagger d_{\mathbf{q}1A\xi\sigma} \rangle$ and $\langle d_{\mathbf{q}1A\xi\sigma}^\dagger d_{\mathbf{q}2B\xi\sigma} \rangle$ entering Eq. (47) are finite even when all symmetries are preserved, as direct calculation demonstrates. For set (ii) we can introduce the same three classes as previously discussed [see Eqs. (41)].

Finally, there is set (iii) of order parameters matrices. It can be presented as

$$\hat{Q} = \hat{U} \text{diag}(\pm i\tilde{\Delta}, q_2, q_3, \pm\Delta) \hat{U}^\dagger, \quad (48)$$

where q_2 can be either real $q_2 = \pm\Delta$, or imaginary $q_2 = \pm i\tilde{\Delta}$. The same is true for q_3 . As we can see, among four eigenvalues of \hat{Q} there is at least one that is purely real, and at least one that is purely imaginary. This condition guarantees that Eq. (48) defines a separate kind of order parameters, which cannot be reduced to two previously defined sets.

As explained in Ref. 24, the order parameter of set (iii) can be split in three groups according to the number of real eigenvalues: the first group represents \hat{Q} 's with one real eigenvalue, the second group is for \hat{Q} 's with two, and the third group is for order parameters with three real eigenvalues. Within each group smaller subdivisions can be introduced, see Table I in Ref. 24. The order parameters in set (iii) shares the features of both density wave states and inter-layer-order states.

V. DISCUSSION

Here we investigated the SU(4)-symmetric model of AB-BLG. Quite remarkably, the obtained self-consistency equation coincides formally with that for the AA-BLG [see Eq. (61) from Ref. 24]. This allows us to use the order parameter classification scheme from the latter paper.

Despite mathematical similarities in the self-consistency equations, there are obvious differences between the two cases. Probably the most obvious one is the difference between electron spectra: AA-BLG demonstrates linear dispersion with a well-defined Fermi surface, while the dispersion is quadratic, with Fermi points, for undoped AB-BLG. The order parameter interpretations are not identical either.

Also, to derive the SU(4)-symmetric form of the interaction Hamiltonian, we assumed that the dipole-dipole interaction can be neglected. Unlike this, for AA-BLG, scattering channels with large transferred momenta (backscattering) were discarded to guarantee the desired symmetry. As a result, the coupling constants entering the self-consistency equations have different physical meanings for two different types of bilayer.

The AB-BLG model with the SU(4) symmetry group was formulated in Ref. 21, whose authors limited the scope to the Hermitian \hat{Q} only. This means that they discussed only the set (i) solutions, and ignored two other possibilities, sets (ii) and (iii). It is quite easy to argue that if \bar{V}_{dir} and \bar{V}_{um} are identical, only Hermitian \hat{Q} are allowed. Indeed, if $\bar{V}_{\text{dir}} = \bar{V}_{\text{um}}$, we obtain from Eq. (30) that $\hat{Q} = \hat{Q}^\dagger$, that is, the order parameter belongs to set (i). Among solutions of this kind there are special case of anomalous quantum Hall states considered in Ref. 21, as well as fractional metal phases, spin, charge, isospin (or valley) density waves and their combinations.

While in our model \bar{V}_{dir} and \bar{V}_{um} are unequal, they are quite close to each other, as Eq. (25) illustrates. Consequently, the characteristic energy scale Δ_+ for set (i) order parameters is much larger than Δ_- for set (ii). Thus, within the SU(4)-symmetric model with Coulomb interaction, the ground state most probably corresponds to a solution from set (i).

The SU(4)-symmetric model offers a convenient framework for classification of the ordered states, as we pointed out in our previous paper²⁴ on AA-BLG. It allows to group numerous non-superconducting order parameters compatible with the AB-BLG electronic structure in three sets, which can be further divided into smaller subsets.

At the same time, the SU(4)-symmetric model results must be treated with caution when experiment is discussed. Indeed, the SU(4)-symmetric model for AB-BLG is an approximation that ignores several non-symmetric contributions, for example, the V^- term in Eq. (15). Figure 1 clearly shows that, while the dipole-dipole coupling constant $V_{\mathbf{k}}^-$ is smaller than $V_{\mathbf{k}}^+$, it is not negligible.

Adding non-SU(4)-symmetric contributions (e.g., dipole-dipole interaction in \hat{H}_{int}), or external perturbations (e.g., magnetic field), or phonons may shift the balance between various ordered phases. Specifically, degeneracy between the states within a given set will be lifted, at least partially. A different, fluctuations-based, mechanism of the degeneracy lifting was investigated in Ref. 21 for set (i) only. These two mechanisms function simultaneously in a real material.

Inclusion of the new terms in the model Hamiltonian may affect the values of the coupling constants. As we discuss in Appendix A, this could have very important consequences for theoretical description of graphene bilayers.

To conclude, we investigated ordered phases of a SU(4)-invariant model for the AB-BLG. Within the framework of the mean field approximation matrix self-consistency equation was derived. It coincides with the self-consistency equation obtained previously for AA-BLG, and demonstrates rich diversity of solutions. Every solution represents a stationary non-superconducting ordered phase of the model. Symmetry-based classification of these orders is discussed.

Appendix A: Coupling constants

Here we discuss the values of the order parameters in the SU(4)-symmetric model of the AB-BLG. Of course, this issue has been addressed in literature. For example, the value of the order parameter was estimated in Ref. 21 as

$$\Delta = \Lambda e^{-2/\lambda\nu_0}, \quad (\text{A1})$$

see the formula beneath Eq. (12) of the latter paper. In this expression Λ is the characteristic band energy $\Lambda \sim t_0$, and the dimensionless product $\lambda\nu_0$ was evaluated as

$$\lambda\nu_0 = \frac{1}{4 \ln 4} \approx 0.18. \quad (\text{A2})$$

This parameter is an analogue of our coupling constant λ_+ . Equation (A2) is based on the RPA calculations in Ref. 26 with $\mathbf{q} = 0$ in the polarization operator [see Eq. (5) there]:

$$\Pi^0 = \frac{2m}{\pi} \ln 4 = \frac{4t_0}{9\pi t^2 a_0^2} \ln 4. \quad (\text{A3})$$

Here $m = q_0^2/2t_0$ denotes an effective electron mass in AB-BLG. Substituting

$$\Lambda = 0.35 \text{ eV}, \quad \frac{\lambda\nu_0}{2} = 0.09, \quad (\text{A4})$$

into (A1), we obtain $\Delta \sim 0.055 \text{ K}$.

We can recover this estimate if we make certain simplifications to our framework. Following Ref. 21, we ignore the momentum-dependence of the interaction

$$V_{\mathbf{q}}^+ \approx V_{\mathbf{q}}^+ \Big|_{\mathbf{q}=0} \approx 26.3t, \quad (\text{A5})$$

see Fig. 1. Under this assumption

$$\bar{V}_{\text{dir}} = \bar{V}_{\text{um}} = \frac{1}{2} V_{\mathbf{q}}^+ \Big|_{\mathbf{q}=0} \approx 13.2t, \quad \Rightarrow \quad \lambda_+ \approx 0.16. \quad (\text{A6})$$

The consistency between the values of λ_+ and $\nu_0\lambda$ from Eq. (A2) is obvious. Using this estimate for λ_+ and Eq. (38), we obtain $\Delta_+ \approx 0.026 \text{ K}$.

The calculated energy scales are very small and inconsistent with typical transition temperatures between different states observed in the AB-BLG samples^{18,27-29}, the latter is tens of Kelvin. The situation becomes more problematic if we realize that the interaction is a decreasing function of the transferred momentum, see Fig. 1. Thus, the estimates in Eq. (A6) are, in fact, upper bounds. If the momentum dependence of the interaction is accounted for, values (25) are derived. As expected, they are smaller than the values in Eq. (A6), which implies even smaller order parameter scale.

This indicates that the SU(4)-symmetric Hamiltonian alone is not sufficient for evaluation of the order parameters. For example, our previous RPA study¹⁵ of the non-SU(4) model for AB-BLG estimates the SDW order parameter as $\Delta^{\text{SDW}} = 4.9 \text{ meV}$, in general consistency with the experimental data. Factors that increase the order parameter in the non-SU(4)-symmetric model are the following. First, in Ref. 15 we took into account the $V_{\mathbf{q}}^-$ interaction term which increases coupling constant λ . Since λ^{-1} is placed in the exponential function, even moderate growth of λ can substantially enhance the transition temperature. Further, in Ref. 15 we used 4-band model of the AB-BLG, and extend the momentum integration in the self-consistency equation to a much larger area in reciprocal space. Effectively this leads to higher pre-exponential factor in the formula for the transition temperature.

Thus, while the SU(4) symmetry of a bilayer graphene model is a useful classification tool, it underestimates order parameter strength.

¹ H. Min, G. Borghi, M. Polini, and A. H. MacDonald, "Pseudospin magnetism in graphene," *Phys. Rev. B* **77**, 041407(R) (2008).

² T. C. Lang, Z. Y. Meng, M. M. Scherer, S. Uebelacker, F. F. Assaad, A. Muramatsu, C. Honerkamp, and S. Wessel, "Antiferromagnetism in the Hubbard Model on the Bernal-Stacked Honeycomb Bilayer," *Phys. Rev. Lett.* **109**, 126402 (2012).

³ Y. Lemonik, I. Aleiner, and V. I. Fal'ko, "Competing nematic, antiferromagnetic, and spin-flux orders in the ground state of bilayer graphene," *Phys. Rev. B* **85**, 245451 (2012).

⁴ M. Kharitonov, "Antiferromagnetic state in bilayer graphene," *Phys. Rev. B* **86**, 195435 (2012).

⁵ Y. Wang, H. Wang, J.-H. Gao, and F.-C. Zhang, "Layer antiferromagnetic state in bilayer graphene: A first-

- principles investigation,” *Phys. Rev. B* **87**, 195413 (2013).
- ⁶ A. L. Rakhmanov, A. V. Rozhkov, A. O. Sboychakov, and F. Nori, “Instabilities of the AA-Stacked Graphene Bilayer,” *Phys. Rev. Lett.* **109**, 206801 (2012).
 - ⁷ Y. Cao, V. Fatemi, A. Demir, S. Fang, S. L. Tomarken, J. Y. Luo, J. D. Sanchez-Yamagishi, K. Watanabe, T. Taniguchi, E. Kaxiras, et al., “Correlated insulator behaviour at half-filling in magic-angle graphene superlattices,” *Nature* **556**, 80 (2018).
 - ⁸ Y. Cao, V. Fatemi, S. Fang, K. Watanabe, T. Taniguchi, E. Kaxiras, and P. Jarillo-Herrero, “Unconventional superconductivity in magic-angle graphene superlattices,” *Nature* **556**, 43 (2018).
 - ⁹ A. O. Sboychakov, A. V. Rozhkov, A. L. Rakhmanov, and F. Nori, “Spin density wave and electron nematicity in magic-angle twisted bilayer graphene,” *Phys. Rev. B* **102**, 155142 (2020).
 - ¹⁰ S. C. de la Barrera, S. Aronson, Z. Zheng, K. Watanabe, T. Taniguchi, Q. Ma, P. Jarillo-Herrero, and R. Ashoori, “Cascade of isospin phase transitions in Bernal-stacked bilayer graphene at zero magnetic field,” *Nat. Phys.* **18**, 771 (2022).
 - ¹¹ H. Zhou, L. Holleis, Y. Saito, L. Cohen, W. Huynh, C. L. Patterson, F. Yang, T. Taniguchi, K. Watanabe, and A. F. Young, “Isospin magnetism and spin-polarized superconductivity in Bernal bilayer graphene,” *Science* **375**, 774 (2022).
 - ¹² A. M. Seiler, F. R. Geisenhof, F. Winterer, K. Watanabe, T. Taniguchi, T. Xu, F. Zhang, and R. T. Weitz, “Quantum cascade of correlated phases in trigonally warped bilayer graphene,” *Nature* **608**, 298 (2022).
 - ¹³ A. O. Sboychakov, A. L. Rakhmanov, A. V. Rozhkov, and F. Nori, “Bilayer graphene can become a fractional metal,” *Phys. Rev. B* **103**, L081106 (2021).
 - ¹⁴ A. L. Rakhmanov, A. V. Rozhkov, A. O. Sboychakov, and F. Nori, “Half-metal and other fractional metal phases in doped AB bilayer graphene,” *Phys. Rev. B* **107**, 155112 (2023).
 - ¹⁵ A. O. Sboychakov, A. V. Rozhkov, and A. L. Rakhmanov, “Triplet superconductivity and spin density wave in biased AB bilayer graphene,” *Phys. Rev. B* **108**, 184503 (2023).
 - ¹⁶ R. S. Akzyanov, A. O. Sboychakov, A. V. Rozhkov, A. L. Rakhmanov, and F. Nori, “AA-stacked bilayer graphene in an applied electric field: Tunable antiferromagnetism and coexisting exciton order parameter,” *Phys. Rev. B* **90**, 155415 (2014).
 - ¹⁷ V. W. Brar, Y. Zhang, Y. Yayan, T. Ohta, J. L. McChes-
ney, A. Bostwick, E. Rotenberg, K. Horn, and M. F. Crommie, “Scanning tunneling spectroscopy of inhomogeneous electronic structure in monolayer and bilayer graphene on SiC,” *Applied Physics Letters* **91**, 122102 (2007).
 - ¹⁸ F. Freitag, M. Weiss, R. Maurand, J. Trbovic, and C. Schönberger, “Homogeneity of bilayer graphene,” *Solid State Communications* **152**, 2053 (2012).
 - ¹⁹ A. Sboychakov, A. V. Rozhkov, K. I. Kugel, and A. L. Rakhmanov, “Phase separation in a spin density wave state of twisted bilayer graphene,” *JETP Letters* **112**, 651 (2020), [*Pis'ma v ZhETPh*, **112**, 693 (2020), in Russian].
 - ²⁰ A. O. Sboychakov, A. V. Rozhkov, A. L. Rakhmanov, and F. Nori, “Antiferromagnetic states and phase separation in doped AA-stacked graphene bilayers,” *Phys. Rev. B* **88**, 045409 (2013).
 - ²¹ R. Nandkishore and L. Levitov, “Quantum anomalous Hall state in bilayer graphene,” *Phys. Rev. B* **82**, 115124 (2010).
 - ²² A. M. Fischer, R. A. Römer, and A. B. Dzyubenko, “Magnetoplasmons and SU(4) symmetry in graphene,” *Journal of Physics: Conference Series* **286**, 012054 (2011).
 - ²³ D. V. Chichinadze, L. Classen, Y. Wang, and A. V. Chubukov, “SU(4) Symmetry in Twisted Bilayer Graphene: An Itinerant Perspective,” *Phys. Rev. Lett.* **128**, 227601 (2022).
 - ²⁴ A. V. Rozhkov, A. O. Sboychakov, and A. L. Rakhmanov, “Ordering in the SU(4)-symmetric model of AA bilayer graphene,” *Phys. Rev. B* **108**, 205153 (2023).
 - ²⁵ A. Rozhkov, A. Sboychakov, A. Rakhmanov, and F. Nori, “Electronic properties of graphene-based bilayer systems,” *Phys. Rep.* **648**, 1 (2016).
 - ²⁶ E. H. Hwang and S. Das Sarma, “Screening, Kohn Anomaly, Friedel Oscillation, and RKKY Interaction in Bilayer Graphene,” *Phys. Rev. Lett.* **101**, 156802 (2008).
 - ²⁷ J. Velasco Jr., L. Jing, W. Bao, Y. Lee, P. Kratz, V. Aji, M. Bockrath, C. Lau, C. Varma, R. Stillwell, et al., “Transport spectroscopy of symmetry-broken insulating states in bilayer graphene,” *Nat. Nano* **7**, 156 (2012).
 - ²⁸ A. Veligura, H. J. van Elferen, N. Tombros, J. C. Maan, U. Zeitler, and B. J. van Wees, “Transport gap in suspended bilayer graphene at zero magnetic field,” *Phys. Rev. B* **85**, 155412 (2012).
 - ²⁹ A. S. Mayorov, D. C. Elias, M. Mucha-Kruczynski, R. V. Gorbachev, T. Tudorovskiy, A. Zhukov, S. V. Morozov, M. I. Katsnelson, V. I. Fal’ko, A. K. Geim, et al., “Interaction-Driven Spectrum Reconstruction in Bilayer Graphene,” *Science* **333**, 860 (2011).